IEEE Access
Multidisciplinary | Rapid Review | Open Access Journal

SPECIAL SECTION ON INNOVATION AND APPLICATION OF INTERNET OF THINGS AND EMERGING TECHNOLOGIES IN SMART SENSING

Received January 7, 2020, accepted January 25, 2020, date of publication February 10, 2020, date of current version February 18, 2020.

Digital Object Identifier 10.1109/ACCESS.2020.2972699

A Smart UAV-Femtocell Data Sensing System for Post-Earthquake Localization of People

ROBERTA AVANZATO AND FRANCESCO BERITELLI
Department of Electrical, Electronics and Computer Engineering, University of Catania, 95125 Catania, Italy
Corresponding author: Francesco Beritelli (francesco.beritelli@dieei.unict.it)

ABSTRACT The paper proposes an intelligent data sensing and geo-localization algorithm, based on an innovative mobile computing system that measures the power level of RF sources through a 2G/5G femtocell-UAV system. In natural disasters (mainly earthquakes and floods) the system can identify any missing persons under the rubble within a range of precision between 1 to 2 meters. In this paper, more specifically, the algorithm allows classifying the terminal even in the presence of obstacles that cause anisotropic propagation of radio signals, through a series of power measurements based on the Reference Signal Received Power (RSRP). An attenuation model that takes into account the different types of materials is introduced, and a method for optimizing the drone's flight path and duration is proposed. The performances, expressed in terms of accuracy in identifying the mobile terminal and in terms of position estimation average error, are evaluated according to the material's density and its attenuation.

INDEX TERMS Femtocell/UAV system, geo-localization technique, 2G/5G radio technologies, reference signal received power (RSRP), mobile terminal classification/positioning algorithm, energy consumption.

I. INTRODUCTION

The recent development of the Internet of Things (IoT), has enabled new types of sensors that can be easily interconnected through the Internet. In the near future, this will have a significant impact on the management of natural disasters (mainly earthquakes and floods), when the aim is improving effectiveness in research, identifying and recovering missing persons, and therefore increasing the possibility of saving lives [1]–[5].

In [6], [7], we proposed an innovative technique for searching and identifying missing persons in natural disaster scenarios by employing a new UAV-femtocell mobile computing system. The algorithm is capable of locating any mobile terminals in any given area monitored through the use of UAV (Unmanned Aerial Vehicle) systems. The idea consists in being able to create coverage through the presence of a femtocell on board a drone, which can then move freely and approach the user terminal, giving the possibility to locate any mobile terminals that may still be working under the rubble.

This paper is concerned with the study of a high-precision (lower than 2 meters) geolocation technique for mobile terminals under the rubble, using a 4G femtocell aboard a drone system. The paper contributes the following:

– a new criterion for classification and geolocation in the presence of non-isotropic radio signal propagation; The algorithm allows to classify the terminal inside or outside the monitoring area and, subsequently, to identify the position with a certain precision, even in the presence of obstacles that act in such a way as to render the radio signal's propagation anisotropic. A complete identification analysis of the terminals under the rubble is proposed in scenarios where the collapsed material represents an anisotropic medium with characteristics that change according to the material's density, the height of the rubble, and the femtocell's transmission power;
– the introduction of a random term that defines the attenuation due to different types of materials and the distance between the terminal and the femtocell;
– a method for optimizing the drone's flight path and duration;
– a post-earthquake scenario simulator that allows to analyze performance when the following parameters vary: debris height, collapsed material density, transmitted power and random attenuation component extra;

The paper is organized as follows: Section 2 briefly summarizes the main localization and positioning techniques,

The associate editor coordinating the review of this manuscript and approving it for publication was Honghao Gao.

followed by section 3 which illustrates the radiomobile signal propagation and material attenuation; Section 4 describes the propounded smart femtocell-UAV data sensing system; Sections 5 and 6 highlight the proposed technique which is divided into two phases: classification, and localization; Section 7 presents a performance analysis in terms of accuracy when identifying the mobile terminal and in terms of position estimation average error; finally Section 8 is devoted to conclusions.

II. STATE OF THE ART ON LOCALIZATION TECHNIQUES

The localization of a mobile terminal by RF signal is a topic often addressed in the literature [8]–[10]. In fact, there are several studies that deal with localizing terminals which are found in disaster areas or more generally in the presence of obstacles, through the analysis and measurement of radio signals. In [11], some different types of attenuation of RF signal were studied. The attenuation of the signal due to the presence of rubble and, therefore, of different types of materials is estimated, considering a signal at 1.8 GHz. The results of this study show, that in a post-earthquake disaster scenario, the losses, compared to free space, are 13dB greater than the losses that occur in an indoor environment, which are equal to about 5 dB.

In [12], the frequency response of the radio channel is studied on different frequency ranges, and the signal attenuation is measured for two types of material: ceramic and brick. First, the 1.8 GHz attenuation is about 4.5 dB more than 900 MHz in the case where the obstacles are arranged evenly around the receiving antenna, and 17.5 dB more when the obstacles are arranged in a less uniform way around the antenna. This implies that a higher frequency signal suffers more attenuation and that the obstacles placed in an irregular manner induce even more attenuation, compared to the case in which they are arranged in a more uniform manner.

Thanks to the features of high mobility and easy deployment, many studies use drones as a means of making on-demand communication services provision possible [13], [14].

More recently, the growing need to connect and cover areas affected by natural disasters has led to the commissioning of multiple studies concerning the use of drone-femtocell systems as an alternative to the classic radio base stations when these are out of service [15]–[19].

In [20], the optimal altitude of the UAV-based base station was analyzed for maximal communication coverage. In [21], an efficient UAV 3D placement with the purpose of maximizing the covered users based on the optimal altitude was proposed. In [22], the authors studied a novel 3D UAV placement with the objective of maximizing the number of covered users according to different requirements of quality of service (QoS).

In these papers, in particular, new solutions are propounded to guarantee coverage and connection to users engaged in rescue operations.

III. RADIOMOBILE SIGNAL PROPAGATION AND MATERIAL ATTENUATION

The transmission of signals in the mobile radio environment is obtained by means of a transmitting antenna, which emits the signal, and a receiving antenna, which receives it.

The mobile terminal, therefore, provides service within the coverage range of a base radio station to which it is docked. In general, the signal can be shielded from the environment, physical obstacles or artefacts limiting the diffusion/propagation of electromagnetic waves.

In particular, three totally different circumstances must be distinguished:

- Signal propagation in a vacuum;
- Signal propagation within the Earth's atmosphere;
- Signal propagation within the Earth's atmosphere and in the presence of materials.

A. SIGNAL PROPAGATION IN A VACUUM

The femtocell generates an electromagnetic wave which in free space presupposes the following properties:

- Isotropic and homogeneous medium;
- Medium without losses;
- Transmission without obstacles or reflections

In this case the only attenuation of the signal is that due to free space, and is expressed by the following formula:

$$A_o = \left(\frac{4\pi d}{\lambda}\right)^2 \tag{1}$$

while the transmission power is given by the Friis's formula:

$$P_T = P_R * G_T * G_R * \left(\frac{\lambda}{4\pi d}\right)^2 \tag{2}$$

where:

- P_T is the power transmitted by the femtocell;
- P_R is the power received from the mobile terminal;
- G_T, G_R are the antenna gains, respectively, in transmission and reception;
- λ is the wavelength of the electromagnetic signal
- d is the distance between antenna in *Tx* and *Rx*.

This formula is not applicable to real cases where there is a non-isotropic medium that attenuates the signal.

B. SIGNAL PROPAGATION WITHIN THE EARTH'S ATMOSPHERE

In this case, the situation is much more complex. Since the air we breathe is neither an isotropic nor a homogeneous medium, and since there are other obstacles (hills, palaces, trees, rain, fog, snow etc.) that shield an electromagnetic radio-mobile signal, the connection is often rendered possible only through reflections and diffractions.

Given that propagation conditions in the atmosphere strongly depend on the type of environment, it is very difficult to find an equation of the trafficking for mobile radio systems since, these waves, are continuously subject to attenuation, dispersion, reflection, refraction and diffraction.

TABLE 1. Attenuation for different obstacle.

Obstacle	Attenuation [dB]
Human Body	3
Cubicles	3 ÷ 5
Window, Brick Wall	2
Brick Wall next to a Metal Door	3
Glass Window	2
Office Window	3
Plasterboard Wall	3
Marble	5
Glass wall with metal frame	6
Dry Wall	4
Office Wall	6
Brick Wall	2 ÷ 8
Concrete Wall	15 ÷ 20
Metal Door	6
Metal Door in brick wall	12 ÷ 13

C. SIGNAL PROPAGATION WITHIN THE EARTH'S ATMOSPHERE AND IN THE PRESENCE OF MATERIALS

In this case, the scenario becomes much more complex, as the propagation takes place in the terrestrial atmosphere, where Friis's formula is no longer valid, and through obstacles made of different types of materials, different shapes and densities.

The study of the signal attenuation effect in presence of different materials has been the subject of numerous scientific publications.

For example, [10], presents a study of the attenuation that a WiFi radio signal undergoes when it crosses various obstacles (panels) of different materials, placed at various distances. It was found that the losses depend on the distance between the transmitter and the panel, as well as the number of panels and panel material.

This dependence has a non-linear character and, therefore, it is difficult to describe it with existing methods of modelling the propagation of radio waves within a transmission medium.

Instead, an overview of the attenuation of some materials that can compose a building is provided in [23]. Also, in this study, the frequency in question is that of the 2.4 GHz WiFi signal. Table 1 demonstrates the attenuation presented by some types of materials.

IV. A SMART FEMTOCELL-UAV DATA SENSING SYSTEM

The elements of the data sensing system proposed in this paper are integrated as shown in Fig. 1.

The system includes a drone with a femtocell aboard and a Raspberry Pi board to locally perform an intelligent analysis of the data, which are subsequently sent to a client (e.g. a tablet) to allow for visual analysis by an operator who determines the coordinates relative to the presence of a mobile terminal.

Considering the power supply and payload this system is fully sustainable, as:

- The drone allows a total payload of 2.5 kg, and a fully programmable control unit;
- The load on the drone is made up of the femtocell (550 g), a power bank to power it (550 g) and a processing unit (100 g), so the total weight of the load is 1.2 kg;

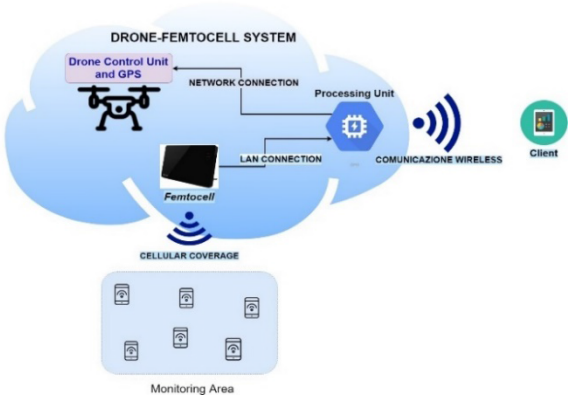

FIGURE 1. Connection/communication scheme of the proposed data sensing system.

- The drone [24] supports the autonomy of 40 minutes with a load of 1.55kg and the amperage 7.67 Ah per battery (it requires 2 batteries);
- Section IV illustrates a fast localization algorithm in which the drone identifies the mobile terminal in less than 30 minutes;
- In the instance of multiple terminals or larger monitoring areas it is necessary to replace the batteries or organize multiple flights with multiple drones.

Considering the functionality of the system, the femtocell receives the power value RSRP (Reference Signal Received Power) measured by the terminal, in a common control channel. The power data, relative to each individual terminal connected, is sent to a single board computer (e.g. Raspberry Pi) via an Ethernet cable connected to the LAN port of the femtocell and to the Ethernet port of the Raspberry.

To obtain information about the points of the area with pre-set GPS coordinates the drone must reach to make power measurements, it is necessary to connect the Raspberry to the drone's GPS coordinate system via network interface. This is how it is possible to associate the position assumed by the drone with the power value that the femtocell receives at that particular point. The data collected at the end of the process are analyzed, the classification algorithm is applied to them, and, subsequently, geolocation is carried out. The analyzed information is subsequently sent to a client via a wireless network generated by the WiFi module inserted in the Raspberry Pi, which also acts as an access point for the clients.

V. CLASSIFICATION ALGORITHM

The first step in identifying missing persons under the rubble is to classify the terminals within the selected monitoring area.

It is therefore assumed that the area in which the collapse occurred was incorporated into a parallelepiped of A_X, A_Y, H_R (length, width and height). Fig. 2 shows the supposed monitoring area.

The hypotheses underlying the classification algorithm are the following:

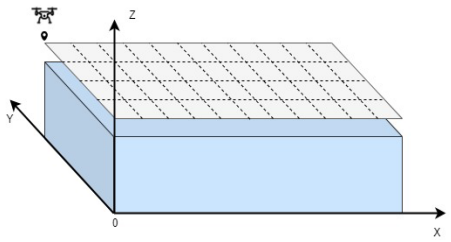

FIGURE 2. Monitoring area.

1. The size of the monitoring area is A_X, A_Y, H_R, meters, the monitoring area is formed by $S = \frac{(A_X * A_Y * H_R)}{27}$ under areas of size $3 \times 3 \times 3$ m^3;
2. The flight of the drone takes place at height H_R, equal to the height of the rubble;
3. The drone takes different positions, which we will indicate with the term "$D_k^{Position}$". The k-th positions are defined at the center of each sub-area S at height Hr with $k = 1, \ldots, (\frac{A_X}{3} * \frac{A_Y}{3})$;
4. The mobile terminals, defined as MS_i for $i = 1, \ldots, S$, are positioned at the points $C_i = (C_i^X, C_i^Y, C_i^Z)$, or in the centroid of the i-th sub area S_i;
5. For each k-th position of the drone, power received by the i-th MS is given by the following formula:

$$P_{i-k} = P_T + G_T + G_R - d_{i-k} * A_0(d_{i-k}) - D_r * d_{i-k} * A_r - r_{i-k} \quad (3)$$

where:

- P_T (dBm) is the transmission power generated by the femtocell; G_T (dB) and G_R (dB) are the antenna gains supposed to be zero;
- d_{i-k} (m) is the distance between the position of each terminal and the k-th position of the femtocell;
- $A_0\,(d_{i-k})$ is the attenuation in dB in free space, a function of the distance of d_{i-k};
- D_r is the density of the material in the interval [0, 1], in the following graphs it will be expressed in percentage [0% ÷ 100%];
- A_r is the material attenuation coefficient [dB/m];
- r_{i-k} is a random value in dB to simulate an additional non-isotropic attenuation between MS_i and $D_k^{Position}$, given by the following formula:

$$r_{i-k} = rand[0, (d_{i-k} * A_r * W * (0.1 + 0.9 * D_r)] \quad (4)$$

where $W = [0,1]$ with default weight of 0.5 (50%).

6. The terminals that will be hooked by the femtocell will be those whose power value will be above a certain threshold, hereinafter referred to as P_{th}:

$$P_{th} = -120[dBm] \quad (5)$$

The connected terminals will therefore be all terminals whose power is greater than P_{th}:
if $P_{i-k} \geq P_{th}$ then $P_{i-k} \in P_{hoocked}$

Once the working hypotheses have been defined and the terminals are generated, it is possible to introduce the classification algorithm. We define the set of terminals hooked P_{hooked}, without repetition and for each position taken by the drone within the monitoring area, such as *{A}*.

Some terminals are hooked by the femtocell but are not internal to the monitoring area, so these terminals represent the "false positive" value. So to reduce false positives it was thought to turn the femtocell around the perimeter of the monitoring area with a distance from the perimeter equal to its coverage radius. This further enables hooking all the terminals present outside the monitoring area, creating the set *{E}*, that is the set of terminals outside the monitoring area.

In the set *{E}* there will be terminals that are also present in the set *{A}*.

Thus the intersection of the two sets creates the set *{X}*. This set is therefore formed by:

$$X = A \cap E \quad (6)$$

The set *{X}* must be subtracted from the set *{A}* to have the set of terminals considered as internal to the monitoring area. Therefore, the set *{I}* is given by:

$$I = A - X \quad (7)$$

Once the terminals inside the monitoring area have been defined, it is possible to proceed to the localization phase.

VI. LOCALIZATION ALGORITHM

The localization phase can be implemented using two different algorithms:

1. Proximity algorithm;
2. Cluster-based fast proximity algorithm.

A. PROXIMITY ALGORITHM

The localization algorithm is based on the hypotheses made previously, in the classification phase.

The localization phase involves estimating the position of the MS_i terminal in the $MS_i^{Estimated}$ point, on the Z plane (in 2D), where this terminal has greater power.

In fact, after defining the terminals classified as IN, having memorized, in the first phase, the P_{i-k} power measurements for each $D_k^{Position}$ it is possible to obtain a power grid in the surface of the monitoring area for each terminal, with which it is possible to estimate the position of the terminal at the grid point where maximum power is obtained for that terminal.

The localization error is expressed in meters and is estimated by calculating the distance between the two vertical axes passing through the positions of MS_i and $D_k^{Position}$ in which the drone measures the maximum power received by the mobile terminal MS_i, then assuming that the error along the Z axis is zero. The error is based on the following formula:

$$\in = d_{vert}[MS_i^{Position}, D_k^{Position}] \quad (8)$$

where $d_{vert}\,(Point_i, Point_k)$ represents the distance between the vertical lines passing through $Point_i$ and $Point_k$.

B. CLUSTER-BASED FAST PROXIMITY ALGORITHM

In the real post-earthquake scenarios of a lost person localization times are very important. It is of fundamental importance to be fast in the rescue times to minimize the drone's energy consumption [25], [26] and that of the mobile devices.

The reduction in flight time and energy consumption has been studied by several researchers. In [27], the propulsion energy consumption model of the fixed-wing UAV was derived and an efficient trajectory maximizing the UAV's energy efficiency was designed.

In addition, energy efficient schemes have attracted wide attention due to the battery technology limitation of mobile devices and UAVs. The authors in [28], studied the minimization problem of the weighted sum energy consumption of the UAV and users. The computation resource scheduling, the bandwidth allocation and the trajectory of the UAV were optimized in the minimization problem.

In this paper the proposed method to reduce energy consumption is based on the optimization of the drone flight. It will be positioned on certain points according to the algorithm that will be hereinafter illustrated.

It is supposed that terminals are not distributed in a non-uniform way within the monitoring area. There will be an area with higher density of terminals unlike another area with lower density. For this reason, it is possible to apply the ''Cluster-based Fast Proximity Algorithm'' to select one subarea, rather than another, where larger quantities of terminals with greater power are detected.

The algorithm includes the following steps:

1. Determination of the minimum resolution of the location error to be obtained (1m, 2m, 3m, etc.);
2. Estimation of the monitoring area so that it can be divided into 4 quadrants for each phase;
3. Selection of 9 grid positions where the drone is stationed. 4 of these positions are represented by the vertices of the monitoring area and another 4 by the median positions of each side, finally the last position is represented by the centroid. From the second phase onwards, the points are reduced to 5 (the middle 4 of the sides of the subarea and the relative centroid);
4. Identification of the number of terminals for each subarea. This is done by evaluating which terminals, at the different points defined above, have the highest power value;
5. Once the number of terminals identified in the various sub-areas has been defined, it is possible to intervene in the point with several terminals and therefore the whole procedure is repeated, starting from point 2, for the sub-area in question;
6. The phases are F and depend on the size of the monitoring area.

The algorithm uses the subdivision in phases for the optimization of the trajectory of the drone, which is defined as ''2'' or ''serpentine''. In particular, hypotheses are made for simplicity:

- The grid must be an MxM matrix in which:

$$M = 2^n + 1 \tag{9}$$

where $n = 2, 3, \ldots, N$;

- The matrix must not be 2×2 or 3×3, since there would be no optimization of the trajectory and therefore no energy/time saving;
- The number of iteration phases of the algorithm must be given by the following formula:

$$F = \log_2 (M - 1) \tag{10}$$

From this formula it can be understood that $n = F$.

Once the initial hypotheses are defined, it is possible to provide a series of definitions:

- E_{tot}^{NO} is the total energy not optimized;
- E_{tot}^{O} is the total energy optimized;
- T_{P-tot}^{NO} is the total non-optimized point processing time;
- T_{P-tot}^{O} is the total point processing time optimized;
- T_{V-tot}^{NO} is the total flight time of the non-optimized drone;
- T_{V-tot}^{O} is the total flight time of the non-optimized drone;
- P it is the power that the drone uses to stay in flight;
- t_p it is the processing time, i.e. the time required for the detection of the power received by the mobile terminal;
- δ_t is the time it takes the drone to fly from one point to another on the grid;

It is now possible to define the non-optimized total energy as:

$$E_{tot}^{NO} = P * (T_{P-tot}^{NO} + T_{V-tot}^{NO}) \tag{11}$$

where:

$$T_{P-tot}^{NO} = t_p * M^2 \tag{12}$$

$$T_{V-tot}^{NO} = \delta_t * (M^2 - 1) \tag{13}$$

While the total optimized energy can be expressed in the following way:

$$E_{tot}^{O} = P * (T_{P-tot}^{O} + T_{V-tot}^{O}) \tag{14}$$

where:

$$T_{P-tot}^{O} = t_p * (5 * F + 4) \tag{15}$$

$$T_{V-tot}^{NO} = \delta_t * \left[2^F * \left(4 + \sum_{F=2}^{F_{MAX}} \frac{2}{2^{F-2}} \right) \right] \tag{16}$$

The flight and total processing time depend on the route iteration phases and on the size of the matrix (also linked with the number of phases). Moreover, to define the previous formulas, we adopted the worst scenario, in which the selected quadrant (in which the terminal is present) is on the opposite side to the last position taken by the drone. Fig. 3 represents an example of the process of iteration and path optimization.

VII. PERFORMANCE EVALUATION

In this section we will illustrate the performance results of the algorithms described above.

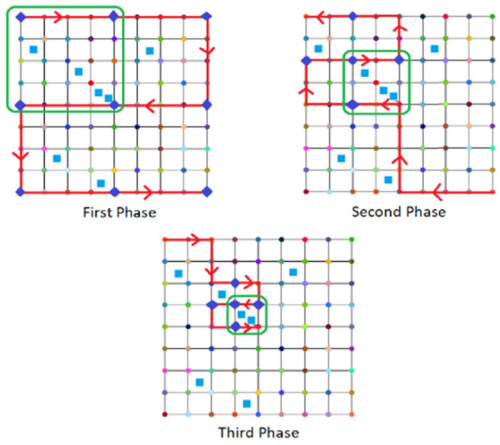

FIGURE 3. Optimized root.

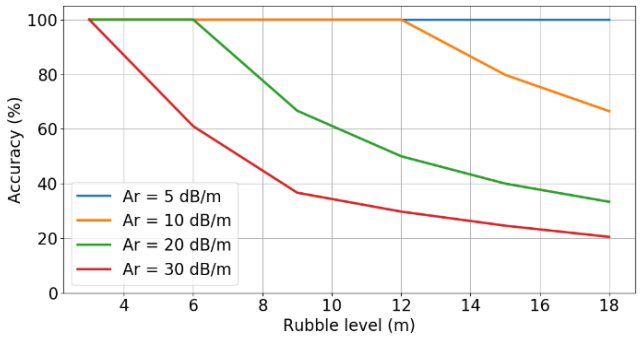

FIGURE 4. Accuracy versus rubble level (*Dr* = 50%).

A. CLASSIFICATION ALGORITHM

As far as the classification phase is concerned, it is possible to evaluate the performance's accuracy to vary some parameters. The hypotheses made for the performance simulation are:

- Area Size: 30×30 m^2
- Weight (W) of 50%
- Transmission power P_T of -57 dBm;
- Power threshold P_{th} of -120 dBm;
- Sub area resolution of 3 m^3

The Fig. 4, 5 and 6 represent the accuracy of the classification as the level of the rubble increases and change respectively A_r, P_T e D_r.

In this graph the density of the material D_r is assumed to be at a value equal to 50% and the curves are shown relatively to the different levels of additional attenuation of the material A_r.

It may be noticed that as the quantity of rubble increases the accuracy visibly decreases, especially, in cases where there is an attenuation due to the material greater than 5 dB/m.

In this graph, obtained by assuming $A_r = 20$ dB/m and the density of the material at 50%,represents the curves relating to the different transmission power levels $P_{t.}$. Also in this case it is clear that accuracy decreases with the increase of rubble, and, in particular, that the curve defined by a transmission power level of -30 dBm decreases more than that relative to the transmission power level equal to -10 dBm.

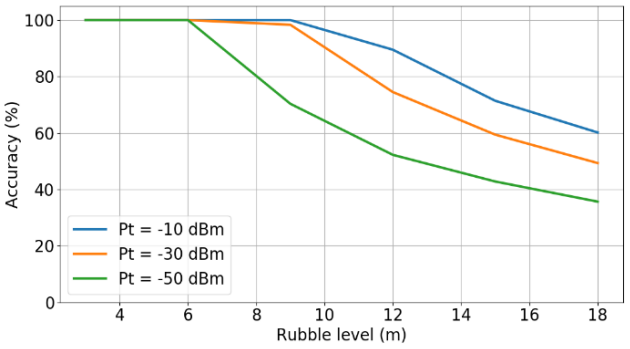

FIGURE 5. Accuracy versus rubble level (*Ar* = 20 dB/m, *Dr* = 50 %).

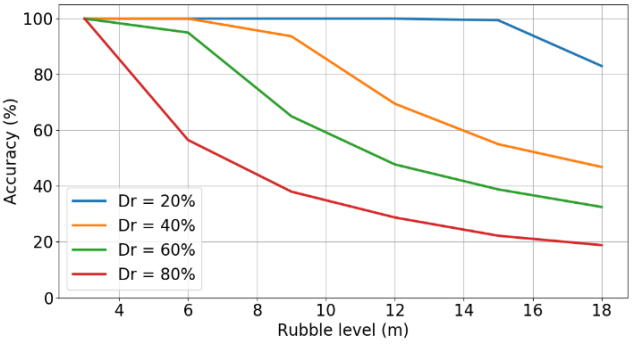

FIGURE 6. Accuracy versus rubble level (*Ar* = 20 dB/m).

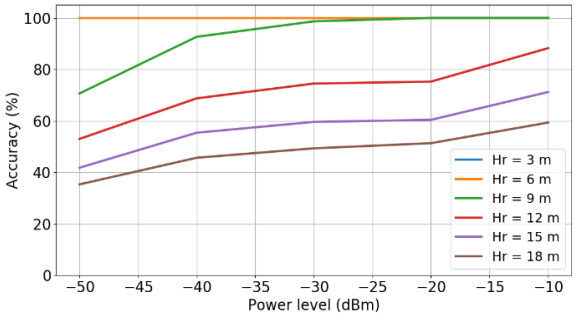

FIGURE 7. Accuracy versus power level (*Ar* = 20 dB/m, *Dr* = 50%).

In this graph, obtained by considering $A_r = 20$ dB/m, the curves are represented as the density of the material D_r changes. Also in this last case the accuracy decreases as the rubble increases, and, particularly, where the density of the material is higher the accuracy will be very low, compared to the case in which the material has lower density. This is because with the same transmission power, with more material, there is more additional attenuation and, therefore, the number of terminals hooked up will be lower.

The Fig. 7, 8 and 9 represent the accuracy of the classification as the level of the transmission signal's strength increases P_T and varies according to H_R, A_r e D_r.

The graph in Fig. 7, obtained by assuming a material density of 50% and a $A_r = 20$ dB/m, the curves are shown relative to the different heights of the rubble. It may be noticed how as the signal power level increases in transmission, the level accuracy grows visibly. In particular, for a drone

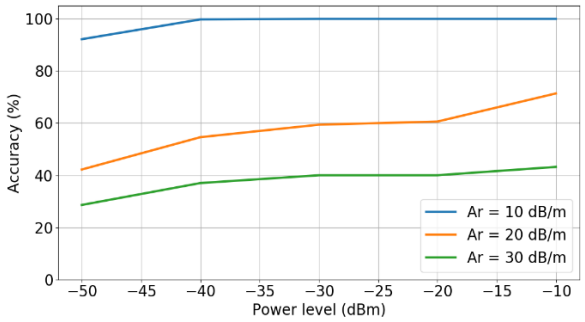

FIGURE 8. Accuracy versus power level ($H_R = 15$ m, $Dr = 50\%$).

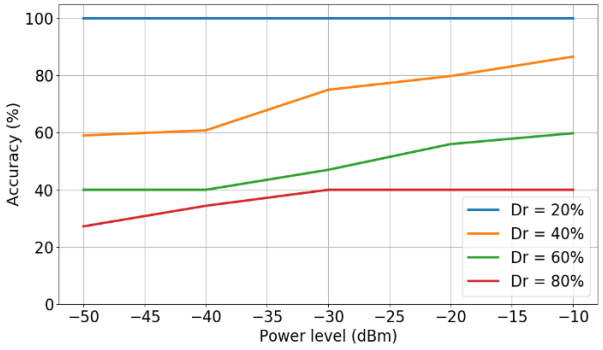

FIGURE 9. Accuracy versus power level ($H_R = 15$ m, $Ar = 20$ dB/m).

height of 3 and 6 meters, accuracy is 100%. This means that the femtocell manages to hook all the terminals present in the monitoring area and classify them as "IN".

The graph in Fig. 8, obtained by assuming the density of the material to be at 50% and the height of the drone A_z at 15m, the curves for the different levels of additional attenuation are represented A_r. Also in this case, it is clear that the accuracy increases with the increase in power, and, in particular, that the curve defined by an attenuation level of 10 dB/m leads to a much higher accuracy than that relative to $A_r = 30$ dB/m.

In Fig. 9, obtained with the hypothesis of $A_r = 20$ dB/m and H_R at 15 m, the curves are represented as the density of the material changes D_r. Also in this last case the accuracy increases with the increase of the power level. In particular, where the density of the material is higher, the accuracy will be very low, compared to the case in which the density of the material is lower, thus, allowing more terminals to be hooked.

Fig. 10 represents the accuracy of the classification as the density of the material increases D_r and to vary the A_r. From the graph it can be seen that by presuming the drone's flight height to be at 15m, accuracy decreases as the density of the material increases and, also, the additional attenuation increases.

B. PROXIMITY ALGORITHM

In this section we will illustrate the performance of the "Proximity Algorithm" to depict the average error of the estimated position.

In Fig. 11, 12 and 13 the average error is represented by varying one of the 3 parameters H_R, P_T and A_r. In Fig. 11 the

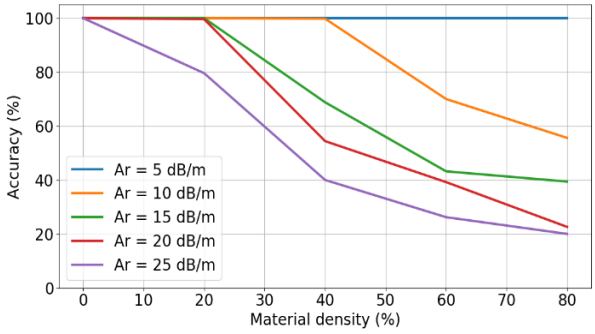

FIGURE 10. Accuracy versus material density ($H_R = 15$ m).

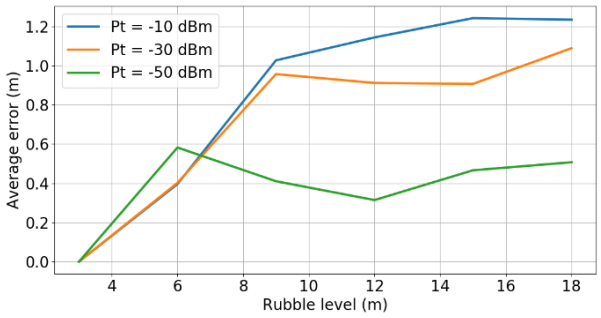

FIGURE 11. Average error versus rubble level ($Ar = 20$ dB/m, $Dr = 50\%$).

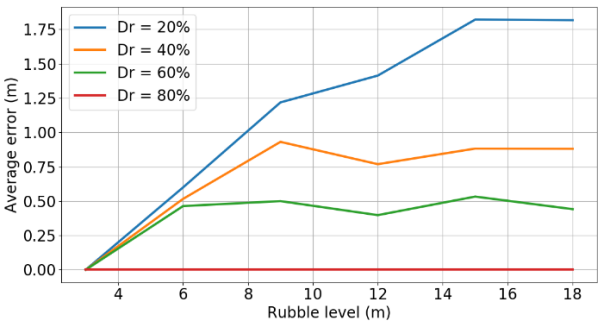

FIGURE 12. Average error versus rubble level and density level ($Ar = 20$ dB/m).

additional attenuation is assumed at 20 dB/m and the density of the material at 50% and the curves relating to different values of P_T are represented. In this case, there is an increase in the average localization error as the rubble increases, and, above all, with incrementing transmission power.

This occurs because as P_T increases, more terminals are hooked on which the localization algorithm must then be performed, so having more terminals, in the presence of attenuation and 50% material density, an error will occur at a higher location, but still between 0 and 1.3m.

In Fig. 12, a material with an attenuation coefficient of 20 dB/m is assumed, and the curves relating to the different levels of material density are represented. Again, in this case, the average error increases as the rubble grows and the material density decreases. The average error decreases as the density of the material increases, because this increase leads to a situation of isotropic attenuation, and, therefore, reduces the localization error.

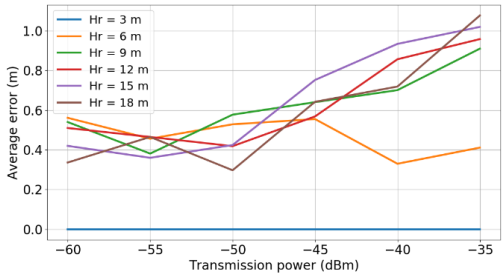

FIGURE 13. Average error versus transmission power ($Ar = 20$ dB/m and $Dr = 50\%$).

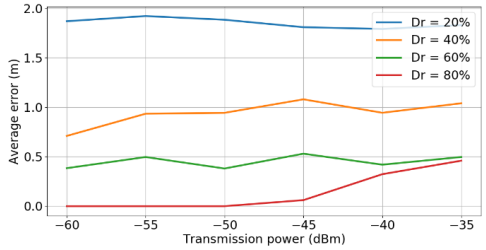

FIGURE 14. Average error versus transmission power and Dr ($Ar = 20$ dB/m, $H_R = 15$m).

Fig. 13 shows the average error as both the transmission power and the Hr increase, assuming an A_r attenuation of 20 dB/m and the density of the material at 50%. As can be seen from the figure, when we are at the height of the rubble at 3m, by varying the transmission power, it is possible to make zero error. As the height of the rubble increases, for transmission powers between [−60 dBm, −50 dBm] there is an error from 40 to 50 cm. For the remaining power values, the average error increases more when we are at different heights. The increase in error as transmission power increases is due to the fact that the femtocell hooks up more terminals, i.e. those deeper down.

Finally, in Fig. 14, as in the previous one, the average error is evaluated as the transmission power increases. In particular, the level of the rubble is assumed to be at 15m and the additional attenuation at 20 dB/m and the curves relating to the different levels of material density are represented.

The average error, in this case, again, increases as the transmitted power increases and the density of the material decreases.

C. CLUSTER-BASED FAST PROXIMITY ALGORITHM

In this subsection we evaluate the performance of the ''Cluster-based fast proximity algorithm''. Placing ourselves in the conditions described in the previous section, in which this algorithm is introduced and illustrated, we show graphs that relate the optimized and non-optimized flight time and to processing time, and therefore also the optimized and non-optimized energy expenditure, to vary of the size of the monitoring area.

Fig. 15, 16 and 17 show that this trajectory optimization algorithm provides considerable energy saving.

Table 2 shows, as the size of the matrix varies, the ''reduction to'' and the ''reduction in'', in percentage, of energy.

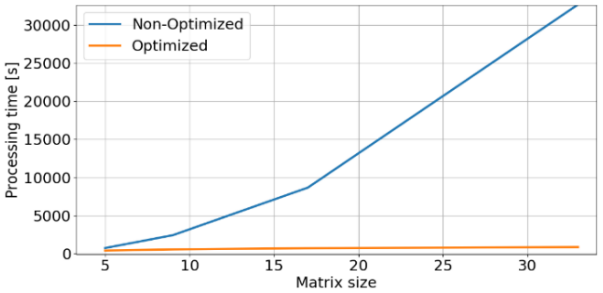

FIGURE 15. Comparison between the curve defined by T^{O}_{P-tot} and T^{NO}_{P-tot}.

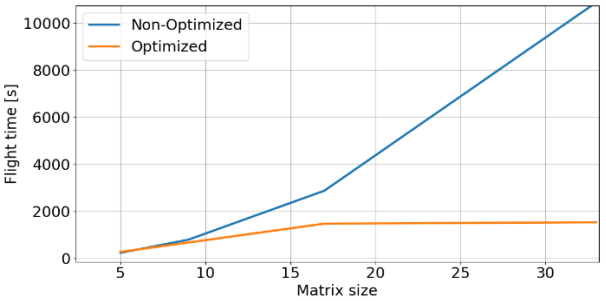

FIGURE 16. Comparison between the curve defined by T^{O}_{V-tot} and T^{NO}_{V-tot}.

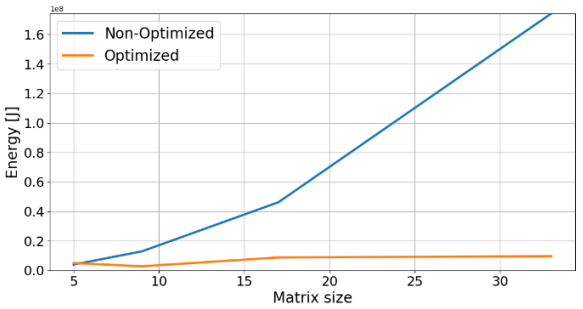

FIGURE 17. Comparison between the curve defined by E^{O}_{tot} and E^{NO}_{tot}.

TABLE 2. Percentage energy optimization.

M	Reduction to [%]	Reduction [%]
5	70,70	29,29
9	38,70	61,30
17	19,05	80,95
33	5,53	94,47

VIII. CONCLUSION

The paper presents a new data sensing system based on an innovative mobile computing system based on the joint use of UAVs and Femtocells. The application for which this study is proposed concerns geolocation, and, therefore, the search for people dispersed in a post-earthquake scenario through an innovative algorithm for coupling mobile terminals. The paper describes, in detail, the classification and geolocation algorithm and presents a performance analysis in terms of accuracy (i.e. number of terminals hooked up) and average error of the estimated position in complex scenarios that take

into account different materials' densities and their attenuation, height of the rubble, transmission power of the femtocell. Considering the typical conditions of a real application scenario, the accuracy obtained is greater than 60% with an average error in estimating the position of about 1 meter.

REFERENCES

[1] C. Luo, J. Nightingale, E. Asemota, and C. Grecos, "A UAV-clouds system for disaster sensing applications," *Proc. IEEE 81st Veh. Technol. Conf. (VTC Spring)*, Glasgow, U.K., May 2015, pp. 1–5, doi: 10.1109/VTCSpring.2015.7145656.

[2] M. Erdelj, M. Król, and E. Natalizio, "Wireless sensor networks and multi-UAV systems for natural disaster management," *Comput. Netw.*, vol. 124, pp. 72–86, Sep. 2017, doi: 10.1016/j.comnet.2017.05.021.

[3] Z. Liu, Y. Chen, B. Liu, C. Cao, and X. Fu, "HAWK: An unmanned mini-helicopter-based aerial wireless kit for localization," *IEEE Trans. Mobile Comput.*, vol. 13, no. 2, pp. 287–298, Feb. 2014, doi: 10.1109/tmc.2012.238.

[4] F. Koohifar, A. Kumbhar, and I. Guvenc, "Receding horizon multi-UAV cooperative tracking of moving RF source," *IEEE Commun. Lett.*, vol. 21, no. 6, pp. 1433–1436, Jun. 2017.

[5] W. Sakpere, M. Adeyeye Oshin, and N. B. W. Mlitwa, "A state-of-the-art survey of indoor positioning and navigation systems and technologies," *South African Comput. J.*, vol. 29, no. 3, pp. 145–197, Dec. 2017, doi: 10.18489/sacj.v29i3.452.

[6] R. Avanzato, F. Beritelli, and M. Vaccaro, "Identification of mobile terminal through femtocell on drone for civil protection applications," in *Proc. 10th IEEE Int. Conf. Intell. Data Acquisition Adv. Comput. Syst., Technol. Appl.*, Metz, France, Sep. 2019, pp. 269–273.

[7] R. Avanzato and F. Beritelli, "An innovative technique for identification of missing persons in natural disaster based on drone-femtocell systems," *Sensors*, vol. 19, no. 20, p. 4547, Oct. 2019, doi: 10.3390/s19204547.

[8] H. Liu, H. Darabai, and J. Liu, "Survey of wireless indoor positioning techniques and systems," *IEEE Trans. Syst., Man, Cybern. C, Appl. Rev.*, vol. 37, no. 6, pp. 1067–1080, Nov. 2007, doi: 10.1109/TSMCC.2007.905750.

[9] S. M. Mehdi Dehghan, S. Haidari, and H. Mordi, "Toward arial simultaneous target localization and obstacle estimation using RSSI observations," in *Proc. 3rd RSI Int. Conf. Robot. Mechatronics (ICROM)*, Tehran, Iran, 2016, pp. 517–522, doi: 10.1109/ICRoM.2015.7367837.

[10] T. Golubeva, Y. Zaitsev, S. Konshin, and I. Duisenbek, "A study on the Wi-Fi radio signal attenuation in various construction materials (obstacles)," in *Proc. 10th Int. Conf. Ubiquitous Future Netw. (ICUFN)*, Prague, Czech Republic, 2018, pp. 718–823, doi: 10.1109/ICUFN.2018.8436785.

[11] J. He, S. Zhou, K. Liao, X. Wei, and E. Li, "Radio frequency propagation characteristics in disaster scenarios," in *Proc. 3rd Asia–Pacific Conf. Antennas Propag.*, Harbin, China, 2014, pp. 818–821, doi: 10.1109/APCAP.2014.6992624.

[12] S. Zhou, K. Liao, J. He, and E. Li, "Investigation of the attenuation characteristics of radio signal in ruins," in *Proc. IEEE Int. Wireless Symp.*, Mar. 2015, pp. 1–4, doi: 10.1109/IEEE-IWS.2015.7164543.

[13] Y. Zeng, R. Zhang, and T. J. Lim, "Wireless communications with unmanned aerial vehicles: Opportunities and challenges," *IEEE Commun. Mag.*, vol. 54, no. 5, pp. 36–42, May 2016, doi: 10.1109/mcom.2016.7470933.

[14] B. Li, Z. Fei, and Y. Zhang, "UAV communications for 5G and beyond: Recent advances and future trends," *IEEE Internet Things J.*, vol. 6, no. 2, pp. 2241–2263, Apr. 2019, doi: 10.1109/jiot.2018.2887086.

[15] M. Deruyck, J. Wyckmans, L. Martens, and W. Joseph, "Emergency ad-hoc networks by using drone mounted base stations for a disaster scenario," in *Proc. IEEE 12th Int. Conf. Wireless Mobile Comput., Netw. Commun.*, New York, NY, USA, Oct. 2016, pp. 1–7, doi: 10.1109/WiMOB.2016.7763173.

[16] M. Deruyck, J. Wyckmans, L. Martens, and W. Joseph, "Designing UAV-aided emergency networks for large-scale disaster scenarios," *J. Wireless Commun. Netw. EURASIP*, vol. 2018, p. 79, Dec. 2018, doi: 10.1186/s13638-018-1091-8.

[17] K. Gomez, A. Hourani, L. Goratti, and R. Riggio, "Capacity evaluation of aerial LTE base-station for public safety communications," in *Proc. Eur. Conf. Netw. Commun. (EuCNC)*, Paris, France, 2015, pp. 133–138, doi: 10.1109/EuCNC.2015.7194055.

[18] J. Lyu, Y. Zeng, R. Zhang, and T. J. Lim, "Placement optimization of UAV-mounted mobile base stations," *IEEE Commun. Lett.*, vol. 21, no. 3, pp. 604–607, Mar. 2017, doi: 10.1109/lcomm.2016.2633248.

[19] E. Kalantari, H. Yanikomeroglu, and A. Yongacoglu, "On the number and 3D placement of drone base stations in wireless cellular networks," in *Proc. IEEE 84th Veh. Technol. Conf. (VTC-Fall)*, Sep. 2016, pp. 1–6, doi: 10.1109/VTCFall.2016.7881122.

[20] A. Al-Hourani, S. Kandeepan, and S. Lardner, "Optimal LAP altitude for maximum coverage," *IEEE Wireless Commun. Lett.*, vol. 3, no. 6, pp. 569–572, Dec. 2014, doi: 10.1109/lwc.2014.2342736.

[21] M. Alzenad, A. El-Keyi, F. Lagum, and H. Yanikomeroglu, "3-D placement of an unmanned aerial vehicle base station (UAV-BS) for energy-efficient maximal coverage," *IEEE Wireless Commun. Lett.*, vol. 6, no. 4, pp. 434–437, Aug. 2017, doi: 10.1109/lwc.2017.2700840.

[22] M. Alzenad, A. El-Keyi, and H. Yanikomeroglu, "3-D placement of an unmanned aerial vehicle base station for maximum coverage of users with different QoS requirements," *IEEE Wireless Commun. Lett.*, vol. 7, no. 1, pp. 38–41, Feb. 2018, doi: 10.1109/lwc.2017.2752161.

[23] *The Basics of Signal Attenuation*. Accessed: Dec. 3, 2019. [Online]. Available: https://www.dataloggerinc.com/wp-content/uploads/2016/11/16_Basics_of_signal_attenuation.pdf

[24] *Technical sheet of MATRIX SERIES 200 V2*. Accessed: Nov. 28, 2019. [Online]. Available: https://www.dji.com/it/matrice-200-series-v2/info#specs

[25] D. Yang, Q. Wu, Y. Zeng, and R. Zhang, "Energy tradeoff in ground-to-UAV communication via trajectory design," *IEEE Trans. Veh. Technol.*, vol. 67, no. 7, pp. 6721–6726, Jul. 2018, doi: 10.1109/tvt.2018.2816244.

[26] F. Wu, D. Yang, L. Xiao, and L. Cuthbert, "Energy consumption and completion time tradeoff in rotary-wing UAV enabled WPCN," *IEEE Access*, vol. 7, pp. 79617–79635, 2019, doi: 10.1109/access.2019.2922651.

[27] Y. Zeng and R. Zhang, "Energy-efficient UAV communication with trajectory optimization," *IEEE Trans. Wireless Commun.*, vol. 16, no. 6, pp. 3747–3760, Jun. 2017, doi: 10.1109/twc.2017.2688328.

[28] X. Hu, K. K. Wong, K. Yang, and Z. Zheng, "UAV-assisted relaying and edge computing: Scheduling and trajectory optimization," *IEEE Trans. Wireless Commun.*, vol. 18, no. 10, pp. 4738–4752, Oct. 2019, doi: 10.1109/TWC.2019.2928539.

ROBERTA AVANZATO received the master's degree in telecommunications engineering from the University of Catania, Italy, in October 2018, where she is currently pursuing the Ph.D. degree in systems, energy, computer, and telecommunications engineering. Since November 2018, she has been a part of the Avionic IoT (AvIoT) project, funded by the MISE (Ministry of Economic Development), she collaborates with the University of Catania on the creation of a platform dedicated to the search for missing persons through the employment of femtocells aboard drones. Her research interests include signal processing, positioning algorithms, and analysis of performance parameters related to the 4G radio channel for high-precision rainfall estimation and monitoring.

FRANCESCO BERITELLI received the master's degree in electronic engineering and the Ph.D. degree in electronics, computer science, and telecommunications engineering from the University of Catania, Catania, Italy, in 1993 and in 1997, respectively. From 1997 to 2000, he was in collaboration with CSELT (now Telecom Italia Lab), took an active part in international ITU-T standardization meetings. Since 2002, he has been an Assistant Professor with the Department of Electric, Electronics and Computer Science Engineering, University of Catania. His main research activities are in the area of robust audio and speech signal classification and recognition, variable bit-rate speech coding, adaptive-rate voice and dual stream transmission for mobile IP telephony applications, QoS in the mobile Internet access, drone communications, cardiac biometric identification, rainfall estimation and monitoring, and post-earthquake geolocation. He has 120 scientific publications, mainly in international journals, books, and conference proceedings.